Inorganic Chemistry

Article

pubs.acs.org/IC

Bimetallic Complexes Supported by a Redox-Active Ligand with Fused Pincer-Type Coordination Sites

Denan Wang, Sergey V. Lindeman, and Adam T. Fiedler*

Department of Chemistry, Marquette University, Milwaukee, Wisconsin 53201, United States

Supporting Information

ABSTRACT: The remarkable chemistry of mononuclear complexes featuring tridentate, meridionally chelating "pincer" ligands has stimulated the development of ligand frameworks containing multiple pincer sites. Here, the coordination chemistry of a novel pentadentate ligand ($\mathbf{L}^{N3O2}$) that provides two closely spaced NNO pincer-type compartments fused together at a central diarylamido unit is described. The trianionic $\mathbf{L}^{N3O2}$ chelate supports homobimetallic structures in which each M(II) ion (M = Co, Cu, Zn) is bound in a meridional fashion by the bridging diarylamido N atom and O,N-donors of the salicyaldimine arms. The metal centers are also coordinated by a mono- or bidentate auxiliary ligand (L^{aux}), resulting in complexes with the general form $[M_2(\mathbf{L}^{N3O2})(L^{aux})_2]^+$ (where L^{aux} = 1-methyl-benzimidazole (1MeBI), 2,2′-bipyridine (bpy), 4,4′-dibromo-2,2′-bipyridine (bpy^{Br2}), or (*S*)-2-(4-isopropyl-4,5-dihydrooxazolyl)pyridine (*S*-^{iPr}OxPy)). The fused nature of the NNO pincer sites results in short metal−metal distances ranging from 2.70 Å for $[Co_2(\mathbf{L}^{N3O2})(bpy)_2]^+$ to 3.28 Å for $[Zn_2(\mathbf{L}^{N3O2})(bpy)_2]^+$, as revealed by X-ray crystallography. The complexes possess C_2 symmetry due to the twisting of the aryl rings of the μ-NAr_2 core; spectroscopic studies indicate that chiral L^{aux} ligands, such as *S*-^{iPr}OxPy, are capable of controlling the helical sense of the $\mathbf{L}^{N3O2}$ scaffold. Since the four- or five-coordinate M(II) centers are linked solely by the amido moiety, each features an open coordination site in the intermetallic region, allowing for the possibility of metal−metal cooperativity in small-molecule activation. Indeed, the dicobalt(II) complex $[Co_2(\mathbf{L}^{N3O2})(bpy^{Br2})_2]^+$ reacts with O_2 to yield a dicobalt(III) species with a μ-1,2-peroxo ligand. The bpy-containing complexes exhibit rich electrochemical properties due to multiple metal- and ligand-based redox events across a wide (3.0 V) potential window. Using electron paramagnetic resonance (EPR) spectroscopy and density functional theory (DFT), it was determined that one-electron oxidation of $[Co_2(\mathbf{L}^{N3O2})(bpy)_2]^+$ results in formation of a $S = 1/2$ species with a $\mathbf{L}^{N3O2}$-based radical coupled to low-spin Co(II) centers.

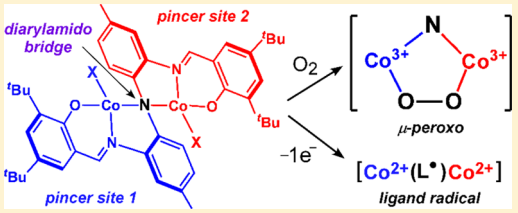

1. INTRODUCTION

Tridentate ligands that coordinate in a meridional fashion are often called pincers due to their rigidity and tightly binding nature.[1] Pincer ligands have found application in nearly all areas of inorganic chemistry, including transition-metal catalysis,[2] sensors,[3] and materials science.[4] While considerable diversity exists within this ever-expanding ligand family, a classic type of pincer features a central diarylamido unit with two flanking phosphine donors (PNP pincers).[5] Several diarylamido-based NNN pincers have also been generated, where the *N*-donor arm is an imine, amine, or heterocyclic donor.[6] Such ligands have been used in the preparation of low-coordinate, yet highly stable, transition-metal complexes capable of performing diverse chemical transformations.

Given the remarkable utility of mononuclear pincer complexes, there has been interest in developing binuclear complexes that contain two pincer-type compartments. The presence of two metal ions offers several catalytic advantages, most crucially the possibility of cooperative action in substrate binding/activation and the ability to perform multiple electron transfers (assuming the metal centers are redox active). A few "bis(pincer)" complexes have been prepared by the dimerization of mononuclear species;[7] in most of these cases, the metal centers are doubly bridged by either the pincer arms[8] or the exogenous ligands not connected to the pincer unit.[9] In other systems, the two metal centers are bridged by pyrazine,[10] 1,4-phenylene,[11] or ferrocene[12] spacers, resulting in metal−metal distances greater than 6 Å. Some groups have connected the pincer compartments by more flexible spacers,[13] thereby allowing the metal centers to approach one another in space. For example, the Ozerov group recently generated a series of ligands in which two PNN pincer units are connected by an alkyl spacer, $(CH_2)_n$ (n = 2 or 4).[14] These ligands were used to prepare hydride-bridged palladium complexes with Pd−Pd distances near 3 Å, as well as a complex featuring a metal−metal bond (Pd−Pd distance of 2.56 Å).

As described in this manuscript, short intermetallic distances can also be achieved by removing the spacer between the two pincer sites entirely. In such "fused" ligands, the two pincer coordination pockets share one of the donor arms, which then serves as the single bridge between the metal centers. This approach to bis(pincer) design has not been widely employed, but Meyer and co-workers reported fused (or "two-in-one") PNN[15] and NNN[16] pincer ligands featuring a bridging pyrazolate that provides one *N*-donor to each ferrous center

Received: June 19, 2015

DOI: 10.1021/acs.inorgchem.5b01380
Inorg. Chem. XXXX, XXX, XXX−XXX

(Figure 1a). Here, we expand upon the fused approach through the synthesis of the novel bis(pincer) ligand $\mathbf{L}^{N3O2}$, shown in

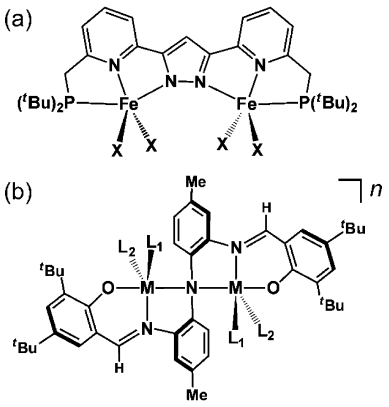

Figure 1. Complexes featuring fused (or "two-in-one") pincer ligands: (a) PNN bis(pincer) ligand recently reported by Meyer and co-workers,[15] and (b) the $\mathbf{L}^{N3O2}$ ligand described in this manuscript.

Figure 1b. Like conventional PNP and NNN pincers, the $\mathbf{L}^{N3O2}$ ligand contains a central diarylamido donor; however, the presence of the two salicyaldimine chelates allows $\mathbf{L}^{N3O2}$ to behave as a binucleating ligand with the diarylamido unit in a bridging position. The resulting framework provides pincer-type coordination to two metal centers in close proximity (3 Å or less).

While not nearly as common as binucleating frameworks with phenolate or pyrazolate bridges, ligands like $\mathbf{L}^{N3O2}$ that feature a bridging diarylamido unit have yielded complexes with attractive electronic and structural properties. For instance, PNP ligands have been used to generate various bimetallic(I) complexes with $M_2(\mu\text{-}NAr_2)_2$ diamond cores (M = Cu,[17] Ni,[18] and Co[19]). Although these complexes utilize PNP ligands, the resulting four-coordinate M(I) centers exist in pseudotetrahedral N_2P_2 environments instead of pincer-like sites. Spectroscopic and computational analysis revealed that the redox chemistry occurs primarily at the bridging N atoms[20]—a finding consistent with previous studies of mononuclear complexes with PNP pincer ligands.[21] The "noninnocent" nature of μ-NAr_2 ligands is a potential asset in catalytic processes requiring multiple electron transfers.[22] Another advantage of diarylamido ligands is their intrinsic chirality due to the relative orientation of the aromatic rings, which gives rise to atropisomers with C_2 symmetry.[14,23] Thus, diarylamido-based ligands could lead to chiral bimetallic complexes for enantioselective catalysis.

To date, the vast majority of bimetallic complexes with bridging diarylamido ligands have featured $M_2(\mu\text{-}NAr_2)_2$ diamond cores.[17−19,24] However, such structures are not ideal for catalysis or small-molecule activation, as the steric bulk of the four phenyl rings limits access to the metal centers. In contrast, the $\mathbf{L}^{N3O2}$ ligand provides a more open framework that preserves three vacant coordination sites on each metal center in a meridional arrangement, similar to mononuclear pincer-based complexes. These open coordination sites are available for the binding of substrates and/or auxiliary ligands (L^{aux}) with advantageous structural or electrochemical properties, as described below. Due to the presence of the salicyaldimine chelates, $\mathbf{L}^{N3O2}$ bears resemblance to binucleating salen and Schiff base ligands that have proven useful in catalysis and materials chemistry.[25] The variable dihedral angle between aryl rings of the amido unit imparts rotational flexibility to the pendant salicyaldimine arms.

In this manuscript, we report the syntheses and X-ray structural characterization of the homobimetallic complexes **1**−**5** indicated in Chart 1. These complexes have the general

Chart 1

General formula: $[M_2(\mathbf{L}^{N3O2})(L^{aux})_2]X$

complex	M	L^{aux}	X
1	Cu	1MeBI	TfO^-
2	Cu	bpy	TfO^-
3	Zn	bpy	TfO^-
4	Co	bpy	ClO_4^-
5	Co	bpy^{Br2}	ClO_4^-
6	Zn	$S\text{-}^{iPr}$OxPy	TfO^-

$S\text{-}^{iPr}$OxPy =

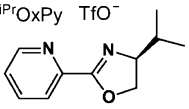

formula $[M_2(\mathbf{L}^{N3O2})(L^{aux})_2]^+$ (M = Co, Cu, Zn), where L^{aux} represents 1-methylbenzimidazole (1MeBI), 2,2′-bipyridine (bpy), or 4,4-dibromo-2,2-bipyridine (bpy^{Br2}). Chiral $[Zn_2(\mathbf{L}^{N3O2})]^+$ frameworks were prepared using the optically active bidentate ligand (*S*)-2-(4-isopropyl-4,5-dihydrooxazolyl)pyridine ($S\text{-}^{iPr}$OxPy; Chart 1). First-row transition metals were selected because of their earth abundance, redox-active nature (except for Zn), and proven ability to perform small-molecule activation. The electrochemical properties of **2**−**5** were thoroughly examined with cyclic and square-wave voltammetries. These bpy-containing complexes exhibit an abundance of electrochemical features arising from both ligand- and metal-based events; indeed, complexes **2** and **4** exhibit six redox events over a potential range of nearly 3.0 V. The electronic structures of $[Co_2(\mathbf{L}^{N3O2})(bpy)_2](ClO_4)$ (**4**) and its one-electron oxidized derivative ($\mathbf{4}^{ox}$) were examined with spectroscopic and computational methods. These results indicate that $\mathbf{4}^{ox}$ is a $S = 1/2$ species in which the μ-NAr_2 unit of the $\mathbf{L}^{N3O2}$ ligand carries a large amount of unpaired spin density. Finally, we demonstrate that $[Co_2(\mathbf{L}^{N3O2})(bpy^{Br2})_2](ClO_4)$ (**5**) reacts with O_2 to yield a dicobalt(III) complex with a bridging peroxo ligand, suggesting that these bimetallic complexes are capable of small-molecule activation.

2. EXPERIMENTAL SECTION

Materials and Physical Methods. Unless otherwise noted, all reagents and solvents were purchased from commercial sources and used as received. Dichloromethane and acetonitrile were purified and dried using a Vacuum Atmospheres solvent purification system. Due to their air-sensitive nature, the dicobalt(II) complexes (**4** and **5**) were handled under inert atmosphere using a Vacuum Atmospheres Omni-Lab glovebox. Elemental analyses were performed at Midwest Microlab, LLC, in Indianapolis, IN.

UV−vis absorption spectra were obtained with an Agilent 8453 diode array spectrometer, and CD spectra were recorded using a Jasco J-715 spectropolarimeter. Infrared (IR) spectra of solid samples were measured with a Thermo Scientific Nicolet iS5 FTIR spectrometer equipped with the iD3 attenuated total reflectance accessory. ^{1}H NMR spectra were collected at room temperature with a Varian 400 MHz spectrometer. EPR experiments were performed using a Bruker ELEXSYS E600 equipped with an ER4415DM cavity, an Oxford Instruments ITC503 temperature controller, and an ESR-900 He flow cryostat. The program EasySpin4 was used to simulate the experimental spectra.[26] Electrochemical measurements were per-

DOI: 10.1021/acs.inorgchem.5b01380
Inorg. Chem. XXXX, XXX, XXX−XXX

formed with an epsilon EC potentiostat (iBAS) under nitrogen atmosphere at a scan rate of 100 mV/s with 0.1 M $(NBu_4)PF_6$ as the electrolyte. A three-electrode cell containing a Ag/AgCl reference electrode, a platinum auxiliary electrode, and a glassy carbon working electrode was employed for voltammetric measurements. Under these conditions, the ferrocene/ferrocenium ($Fc^{+/0}$) couple has an $E_{1/2}$ value of +0.47 V in MeCN.

Bis(4-methyl-2-nitrophenyl)amine. This procedure was adapted from previously published reports.[27] A round-bottom flask equipped with a stir bar was charged with a mixture of concentrated nitric acid (70%; 10 mL) and glacial acetic acid (45 mL). The mixture was cooled to 0 °C, and bis(4-methylphenyl)amine (5.00 g, 25.4 mmol, 1.0 equiv) was added. The yellow mixture was stirred for 10 min in an ice/water bath before dropwise addition of isoamyl nitrite (8.75 g, 75 mmol, 3.0 equiv) over the course of 5 min. The solution turned to dark green; after stirring for an additional 10 min, the solution changed to an orange color and a precipitate started to form. The orange precipitate was collected via filtration, washed with diethyl ether, and dried under vacuum (6.45 g, 22.5 mmol, 89% yield). ^{1}H NMR (400 MHz, $CDCl_3$) δ: 2.37 (s, 6H, CH_3), 7.32 (d, J = 8.5 Hz, 2H, ArH), 7.42 (d, J = 8.5 Hz, 2H, ArH), 7.99 (s, 2H, ArH), 10.80 (s, 1H, NH). ^{13}C NMR (101 MHz, $CDCl_3$) δ: 20.43, 119.73, 125.25, 126.33, 131.73, 135.19, 135.85.

Bis(4-methyl-2-aminophenyl)amine. A 250 mL pressure vessel equipped with a stir bar was filled with solid bis(4-methyl-2-nitrophenyl)amine (3.00 g, 10.45 mmol, 1.0 equiv), MeOH (100 mL), and 10% Pd/C (500 mg, 0.47 mmol, 0.0045 equiv). The flask was pressurized with H_2 gas (46 psi), and the mixture was stirred at 65 °C for 4 h, during which the bright orange solution became colorless. The mixture was filtered through Celite and washed with cold MeOH, and the solvent was removed under vacuum to yield a light purple oil. The oil residue was triturated with Et_2O (20 mL) to give a pale brown powder, which was collected by filtration and dried under vacuum (2.25 g, 9.93 mmol, 95% yield). ^{1}H NMR (300 MHz, $CDCl_3$) δ: 2.25 (s, 6H, CH_3), 3.56 (s, 4H, NH_2), 4.80 (s, 1H, NH), 6.54 (d, J = 7.9 Hz, 2H, ArH), 6.63−6.58 (m, 4H, ArH). ^{13}C NMR (75 MHz, $CDCl_3$) δ: 21.14, 109.99, 117.27, 120.49, 129.10, 133.11, 138.61.

Pro-Ligand H_3L^{N3O2}. To a solution of bis(4-methyl-2-aminophenyl)amine (454 mg, 2.0 mmol, 1.0 equiv) in MeOH (30 mL) was added 3,5-di-*tert*-butyl-2-hydroxybenzaldehyde (937.3 mg, 4.0 mmol, 2.0 equiv) and 5 drops of formic acid. The mixture was heated overnight at 60 °C under an inert atmosphere, giving rise to a bright yellow precipitate. The yellow solid was collected by filtration and dried under vacuum to yield pure H_3L^{N3O2} as a yellow powder (1.20 g, 1.82 mmol, 91% yield). X-ray-quality crystals were obtained by slow evaporation of a H_3L^{N3O2} solution in a mixture of CH_2Cl_2:CH_3OH (9:1). Anal. Calcd for $C_{44}H_{57}N_3O_2$ (M_W = 659.96 g mol^{-1}): C, 80.08; H, 8.71; N, 6.37. Found: C, 80.32; H, 8.89; N, 6.27. ^{1}H NMR (400 MHz, $CDCl_3$) δ: 1.17 (s, 18H, C(CH_3)$_3$), 1.30 (s, 18H, C(CH_3)$_3$), 2.35 (s, 6H, CH_3), 6.55 (s, 1H, NH), 6.99 (s, 2H, ArH), 7.02 (d, J = 8.2 Hz, 2H, ArH), 7.17 (s, 2H, ArH), 7.36−7.30 (m, 4H, ArH), 8.64 (s, 2H, ArH), 13.26 (s, 2H, N=C-H). ^{13}C NMR (101 MHz, $CDCl_3$) δ: 20.79, 29.13, 31.46, 34.11, 34.81, 116.46, 118.56, 119.27, 126.75, 127.78, 127.89, 130.44, 134.26, 136.82, 138.47, 140.22, 158.15, 163.94.

*[Cu_2(L^{N3O2})(1MeBI)$_2$](OTf) (**1**).* The pro-ligand H_3L^{N3O2} (66.0 mg, 0.100 mmol), 1MeBI (26.4 mg, 2.0 equiv), and $Cu(OTf)_2$ (72.3 mg, 2.0 equiv) were added to a 25 mL flask containing MeCN (5 mL). After stirring for 5 min, NEt_3 (42 μL, 3.0 equiv) was added, causing the solution to turn from brown to reddish brown. The mixture was stirred for 2 h and then filtered through Celite. A small amount of MeOH (1 mL) was slowly added to the filtrate, and the resulting solution was allowed to slowly evaporate over the course of 2 days. This process yielded orange-brown crystals that were collected, washed with Et_2O (3 mL), and dried under vacuum. Yield = 65 mg (54%). X-ray-quality crystals were grown from a concentrated 1:1 solution of CH_2Cl_2:MeOH. The resulting structure revealed uncoordinated MeOH molecules in the asymmetric unit, and elemental analysis suggests that a small amount (~1.0 equiv) remains after drying. Anal. Calcd for $C_{61}H_{70}Cu_2F_3N_7O_5S{\cdot}CH_3OH$ (M_W = 1229.4 g mol^{-1}): C, 60.56; H, 6.07; N, 7.97. Found: C, 60.35; H, 5.69; N, 7.82. UV−vis [λ_{max}, nm (ε, M^{-1} cm^{-1}) in MeCN]: 310 (19 000), 424 (13 100). FTIR (cm^{-1}; solid): 2953 (m), 2903 (w), 2864 (w), 1593 (m), 1523 (m), 1493 (m), 1456 (m), 1420 (m), 1358 (s), 1151 (s). ^{19}F NMR (δ, CD_3CN): −79.3 (OTf). ^{1}H NMR (δ, CD_3CN): −30.6 (2H), 1.4 (18H), 2.2 (18H), 4.0 (6H), 6.2 (2H), 7.5 (2H), 8.8 (2H), 16.2 (2H), 22.7 (2H), 30.5 (2H), 40.2 (2H), 41.8 (6H), 51.7 (2H). μ_{eff} = 2.41 μ_B (Evans method).

*[Cu_2(L^{N3O2}) (bpy)$_2$](OTf) (**2**).* The procedure was nearly identical to the one used to prepare complex **1**; the only difference was the replacement of 1MeBI with bpy (31.2 mg, 2.0 equiv). Yield = 104 mg (84%). Anal. Calcd for $C_{65}H_{70}Cu_2F_3N_7O_5S$ (M_W = 1245.4 g mol^{-1}): C, 62.68; H, 5.67; N, 7.87. Found: C, 62.46; H, 5.73; N, 7.85. UV−vis [λ_{max}, nm (ε, M^{-1} cm^{-1}) in MeCN]: 298 (40 200), 430 (15 100), 495 (sh). FTIR (cm^{-1}; solid): 2948 (m), 2904 (w), 2863 (w), 1593 (m), 1521 (m), 1489 (m), 1352 (s), 1152 (s). ^{19}F NMR (δ, CD_3CN): −79.3 (OTf). ^{1}H NMR (δ, CD_3CN): −29.5 (2H), 1.4 (18H), 2.8 (18H), 8.9 (2H), 9.6 (2H), 10.1 (2H), 12.9 (4H), 13.3 (2H), 18.1 (2H), 25.9 (2H), 33.6 (2H), 36.0 (2H), 39.9 (6H), 45.1 (2H), 116.0 (2H). μ_{eff} = 2.36 μ_B (Evans method).

*[Zn_2(L^{N3O2}) (bpy)$_2$](OTf) (**3**).* To a 25 mL flask were added the pro-ligand H_3L^{N3O2} (66.0 mg, 0.100 mmol), 2,2′-bipyridine (31.2 mg, 2.0 equiv), and $Zn(OTf)_2$ (72.7 mg, 2.0 equiv). The components were dissolved in a 1:1 mixture of MeCN:CH_2Cl_2 (5 mL) and stirred for 5 min. The addition of NEt_3 (42 μL, 3.0 equiv) caused the solution to turn to an orange color. The mixture was stirred overnight and filtered through Celite, and the solvent was removed under vacuum. The resulting powder was washed with Et_2O (5 mL), dried under vacuum, and dissolved in a 1:1 mixture of MeCN:MeOH (4 mL). Slow evaporation over the course of 2 days provided orange crystals that were collected via filtration, washed with Et_2O, and dried under vacuum. Yield = 96 mg (77%). Orange crystals, suitable for X-ray diffraction, were grown from a concentrated 1:1 solution of CH_2Cl_2:MeOH. Anal. Calcd for $C_{65}H_{70}F_3N_7O_5SZn_2$ (M_W = 1249.1 g mol^{-1}): C, 62.50; H, 5.65; N, 7.85. Found: C, 62.16; H, 5.60; N 7.76. UV−vis [λ_{max}, nm (ε, M^{-1} cm^{-1}) in MeCN]: 425 (24 300), 460 (19 600). FTIR (cm^{-1}; solid): 2949 (m), 2904 (w), 2865 (w), 1598 (m), 1523 (m), 1487 (m), 1379 (s), 1159 (s). ^{19}F NMR (δ, CD_3CN) δ: −79.4 (OTf). ^{1}H NMR (δ, CD_3CN): 1.11 (s, 18H, C(CH_3)$_3$), 1.37 (s, 18H, C(CH_3)$_3$), 2.13 (s, 6H, CH_3), 5.54 (d, J = 8.3 Hz, 2H, L^{N3O2}-ArH), 6.17 (d, J = 8.3 Hz, 2H, L^{N3O2}-ArH), 7.03 (s, 2H, L^{N3O2}-ArH), 7.21 (dd, J = 8.1, 5.5 Hz, 2H, bpy-ArH), 7.26 (d, J = 2.7 Hz, 2H, L^{N3O2}-ArH), 7.39 (d, J = 2.7 Hz, 2H, L^{N3O2}-ArH), 7.45−7.51 (m, 2H, bpy-H), 7.96 (d, J = 8.1 Hz, 2H, bpy-H), 7.99−8.07 (m, 8H, bpy-H), 8.48 (s, 2H, N=C-H), 8.75 (d, J = 6.3 Hz, 2H, bpy-H).

*[Co_2(L^{N3O2}) (bpy)$_2$](ClO$_4$) (**4**).* The procedure was identical to the one used to prepare complex **3**, except for the substitution of $Co(ClO_4)_2{\cdot}6H_2O$ (73.2 mg, 2.0 equiv) for $Zn(OTf)_2$. Yield = 85 mg (71%). Brown crystals, suitable for X-ray diffraction, were grown from a concentrated 1:1 solution of acetone:MeOH. Anal. Calcd for $C_{64}H_{70}ClCo_2N_7O_6$ (M_W = 1186.6 g mol^{-1}): C, 64.78; H, 5.95; N, 8.26. Found: C, 62.37; H, 5.86; N, 7.91 (the discrepancies are due to small amounts of $[HNEt_3]ClO_4$ salt, which persists even after multiple recrystallizations). UV−vis [λ_{max}, nm (ε, M^{-1} cm^{-1}) in MeCN]: 440 (13 800), 590 (sh). FTIR (cm^{-1}; solid): 2956 (m), 2904 (w), 2867 (w), 1587 (m), 1511 (m), 1441 (m), 1360 (s), 1162 (m). ^{1}H NMR (δ, CD_3CN): 0.74 (s, 18H, C(CH_3)$_3$), 1.30 (s, 18H, C(CH_3)$_3$), 2.09 (s, 6H, CH_3), 5.48 (d, J = 8.4 Hz, 2H, L^{N3O2}-ArH), 6.13 (d, J = 8.4 Hz, 2H, L^{N3O2}-ArH), 7.01 (s, 2H, L^{N3O2}-ArH), 7.15 (d, J = 2.4 Hz, 2H, L^{N3O2}-ArH), 7.23 (d, J = 2.4 Hz, 2H, L^{N3O2}-ArH), 7.34 (t, J = 6.0 Hz, 2H, bpy-H), 7.68 (t, J = 6.0 Hz, 2H, bpy-H), 7.73 (s, 2H, N=C-H), 7.84 (d, J = 6.0 Hz, 2H, bpy-H), 7.96−8.12 (m, 6H, bpy-H), 8.18 (d, J = 7.9 Hz, 2H, bpy-H), 10.23 (d, J = 6.0 Hz, 2H, bpy-H).

*[Co_2(L^{N3O2}) (bpy^{Br2})$_2$](ClO$_4$) (**5**).* This complex was prepared in the same manner as complexes **3** and **4**, with the exception that bpy^{Br2} (62.8 mg, 2.0 equiv) was used as the auxiliary ligand. Yield = 86 mg (57%). The X-ray structure revealed two uncoordinated MeOH molecules in the asymmetric unit. Anal. Calcd for $C_{64}H_{66}Br_4ClCo_2N_7O_6{\cdot}2CH_3OH$ (M_W = 1566.3 g mol^{-1}): C, 50.61; H, 4.76; N, 6.26. Found: C, 48.98; H, 4.48; N, 6.31 (the discrepancies

DOI: 10.1021/acs.inorgchem.5b01380
Inorg. Chem. XXXX, XXX, XXX−XXX

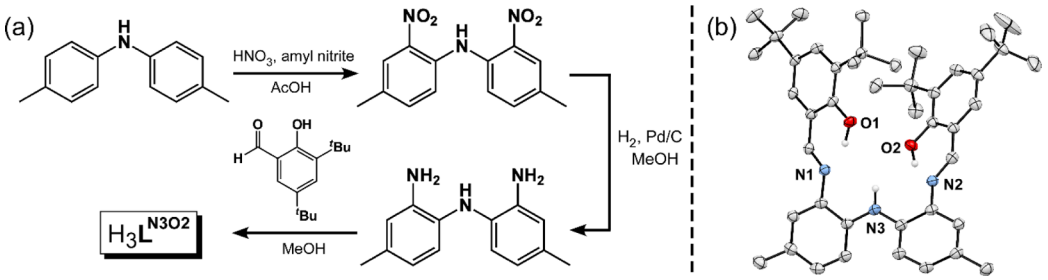

Figure 2. (a) Synthetic route for the pro-ligand H_3L^{N3O2}. (b) Molecular structure of H_3L^{N3O2} determined by X-ray crystallography (50% probability thermal ellipsoids).

are due to small amounts of $[HNEt_3]ClO_4$ salt). UV−vis [λ_{max}, nm (ε, M^{-1} cm^{-1}) in MeCN]: 260 (30 000), 340 (14 900), 420 (8900), 580 (sh). FTIR (cm^{-1}; solid): 3070 (w), 2948 (m), 2900 (w), 2863 (w), 1589 (m), 1543 (w), 1520 (m), 1492 (w), 1462 (m), 1397 (m), 1251 (m), 1170 (m). ^{1}H NMR (δ, CD_3CN): 0.77 (s, 18H, $C(CH_3)_3$), 1.31 (s, 18H, $C(CH_3)_3$), 2.17 (s, 6H, CH_3), 5.62 (d, J = 8.2 Hz, 2H, L^{N3O2}-Ar*H*), 6.23 (d, J = 8.2 Hz, 2H, L^{N3O2}-Ar*H*), 7.10 (s, 2H, L^{N3O2}-Ar*H*), 7.17 (d, J = 2.5 Hz, 2H, L^{N3O2}-Ar*H*), 7.30 (d, J = 2.5 Hz, 2H, L^{N3O2}-Ar*H*), 7.57 (dd, J = 6.0, 1.9 Hz, 2H, bpy-*H*), 7.65 (d, J = 6.0 Hz, 2H, bpy-*H*), 7.80 (s, 2H, N=C-*H*), 7.92 (dd, J = 6.3, 1.9 Hz, 2H, bpy-*H*), 8.27 (d, J = 1.9 Hz, 2H, bpy-*H*), 8.46 (d, 2H, J = 1.9 Hz, bpy-*H*), 9.95 (d, J = 6.3 Hz, 2H, bpy-*H*).

*$[Co_2(O_2)(L^{N3O2})(bpy^{Br2})_2](ClO_4)$ (**5-O$_2$**).* Complex **5** was dissolved in a 1:1 mixture of CH_2Cl_2:MeOH and exposed to air. Slow evaporation over the course of several days provided dark brown crystals of both **5** and **5-O$_2$** that were collected via filtration, washed with Et_2O, and dried under vacuum. Attempts to separate the two complexes were unsuccessful. Regardless, the spectroscopic features of **5-O$_2$** were distinguished by comparison to data collected with pure samples of **5**. FTIR (cm^{-1}; solid): 2948 (m), 2899 (w), 2863 (w), 1588 (m), 1543 (w), 1518 (m), 1493 (m), 1462 (m), 1398 (m), 1252 (m), 1170 (m), 1080 (s). ^{1}H NMR (δ, CD_3CN): 0.77 (s, 18H, $C(CH_3)_3$), 1.36 (s, 18H, $C(CH_3)_3$), 2.32 (s, 6H, CH_3), 5.63 (d, J = 8.4 Hz, 2H, L^{N3O2}-Ar*H*), 6.55 (d, J = 8.4 Hz, 2H, L^{N3O2}-Ar*H*), 7.17 (d, J = 6.4 Hz, 2H, bpy-*H*), 7.35 (d, J = 2.4 Hz, 2H, L^{N3O2}-Ar*H*), 7.37 (dd, J = 6.4, 2.0 Hz, 2H, bpy-*H*), 7.63 (d, J = 2.4 Hz, 2H, L^{N3O2}-Ar*H*), 7.70 (d, J = 2.0 Hz, 2H, bpy-*H*), 8.34 (dd, J = 6.1, 1.9 Hz, 2H, bpy-*H*), 8.37 (d, J = 1.9 Hz, 2H, bpy-*H*), 8.45 (s, 2H, L^{N3O2}-Ar*H*), 8.61 (s, 2H, N=C-*H*), 9.00 (d, J = 6.1 Hz 2H, bpy-*H*).

*$[Zn_2(L^{N3O2})(S\text{-}^{iPr}OxPy)_2](OTf)$ (**6**).* To a 25 mL flask were added the pro-ligand H_3L^{N3O2} (66.0 mg, 0.100 mmol), $Zn(OTf)_2$ (72.7 mg, 2.0 equiv), and *S*-^{iPr}OxPy (38 mg, 2.0 equiv). The components were dissolved in a 3:1 mixture of MeCN:CH_2Cl_2 (8 mL) and stirred for 5 min. The addition of NEt_3 (42 μL, 3.0 equiv) caused the yellow solution to turn to a red-orange color. The mixture was stirred for 1 h and filtered through Celite, and the solvent was removed under vacuum. The resulting powder was washed with pentane (5 mL) and dried under vacuum. Yield = 73.2 mg (56%). Anal. Calcd for $C_{67}H_{82}F_3N_7O_7SZn_2$ (M_W = 1317.2 g mol^{-1}): C, 61.09; H, 6.27; N, 7.44. Found: C, 60.79; H, 5.81; N, 7.97 (the slight discrepancies are due to small amounts of NEt_3). UV−vis [λ_{max}, nm (ε, M^{-1} cm^{-1}) in MeCN]: 420 (21 000), 460 (18 300). FTIR (cm^{-1}; solid): 3055 (w), 2953 (m), 2906 (w), 2867 (w), 1653 (w), 1606 (m), 1591 (m), 1523 (m), 1487 (m), 1402 (m), 1236 (s), 1153 (s). ^{19}F NMR (δ, CD_3CN): −79.4. ^{1}H NMR (δ, CD_3CN): 0.52 (d, J = 6.8 Hz, 6H, $CH(CH_3)_2$), 0.59 (d, J = 6.8 Hz, 6H, $CH(CH_3)_2$), 1.11 (s, 18H, $C(CH_3)_3$), 1.36 (s, 18H, $C(CH_3)_3$), 1.56−1.62 (m, 2H, $CH(CH_3)_2$), 2.22 (s, 6H, CH_3), 3.92−3.82 (m, 2H, oxazol-*H*), 4.48 (dd, J = 9.4, 6.9 Hz, 2H, oxazol-*H*), 4.65 (t, J = 9.4 Hz, 2H, oxazol-*H*), 6.80 (d, J = 8.2 Hz, 2H, L^{N3O2}-Ar*H*), 6.89 (d, J = 8.2 Hz, 2H, L^{N3O2}-Ar*H*), 6.93 (s, 2H, L^{N3O2}-Ar*H*), 7.12 (d, J = 2.7 Hz, 2H, L^{N3O2}-Ar*H*), 7.16 (dd, J = 7.9, 5.0 Hz, 2H, py-*H*), 7.40 (d, J = 2.7 Hz, 2H, L^{N3O2}-Ar*H*), 7.57 (d, J = 7.9 Hz, 2H, py-*H*), 7.98 (t, J = 7.9 Hz, 2H, py-*H*), 8.10 (s, 2H, N=C-*H*), 8.58 (d, J = 5.0 Hz, 2H, py-*H*).

Crystallographic Studies. X-ray diffraction data were collected at 100 K with an Oxford Diffraction SuperNova diffractometer equipped with a 135 mm Atlas CCD detector and Cu Kα radiation source. The resulting data were processed with the CrysAlis Pro program package (Agilent Technologies, 2011). An absorption correction was performed on the real crystal shape followed by an empirical multiscan correction using SCALE3 ABSPACK routine. Structures were solved using the SHELXS program and refined with the SHELXL program[28] within the Olex2 crystallographic package.[29] All non-hydrogen atoms were refined with anisotropic displacement parameters. Hydrogen atoms were generally positioned geometrically and refined using appropriate geometric restrictions on bond lengths and bond angles within a riding/rotating model, and the torsion angles of $-CH_3$ hydrogens were optimized to better fit residual electron density. For complexes **1**, **3**, and **5-O$_2$**, the unit cells contained large void spaces filled with heavily disordered solvent, and exact localization of these molecules was not feasible. The solvent-mask procedure implemented in Olex2 was therefore applied to account for the contribution of these solvent molecules to diffraction intensities. X-ray crystallographic parameters are provided in Table S1, and experimental details are available in the CIFs.

DFT Computations. DFT calculations were carried out using the ORCA 2.9 software package developed by Dr. F. Neese (MPI for Chemical Energy Conversion).[30] When X-ray structures were not available (**4^{ox}** and **6**), computational models were generated via geometry optimizations that employed the Becke-Perdew (BP86) functional.[31] The computational models of **4** and **4^{ox}** omitted the *tert*-butyl substituents of the phenolate donors. Calculations of the four possible isomers of **6**, however, involved the entire complex without modification of the L^{N3O2} or *S*-^{iPr}OxPy ligands. Once the optimized models were obtained, molecular energies and electronic structure parameters were calculated using Becke's three-parameter hybrid functional for exchange along with the Lee−Yang−Parr correlation functional (B3LYP).[32] All calculations utilized Ahlrichs' valence triple-ζ basis set (TZV) and TZV/J auxiliary basis set in conjunction with polarization functions on all atoms.[33] Solvent effects were calculated using the conductor-like screening model (COSMO)[34] with a dielectric constant (ε) of 36.6 for MeCN. Exchange coupling constants (J) were obtained using Noodleman's broken symmetry approach ($H = -2JS_A \cdot S_B$).[35] Isosurface plots of molecular orbitals were prepared with Laaksonen's gOpenMol program.[36]

3. RESULTS AND DISCUSSION

3.A. Synthesis of H_3L^{N3O2} and Bimetallic Complexes. The pro-ligand H_3L^{N3O2} is prepared by the route shown in Figure 2. The final step in the synthesis is the condensation of bis(2-amino-4-methylphenyl)amine with 2 equiv of 3,5-di-*tert*-butylsalicylaldehyde. Formation of the two salicyaldimine units required the presence of *tert*-butyl groups on the phenol ring. Salicylaldehydes with less bulky substituents reacted instead with the central diarylamine moiety to give a cyclized 2-(benzimidazol-2-yl)phenol product (Figure S1). The identity of H_3L^{N3O2} was confirmed by ^{1}H NMR and X-ray crystallography. In the solid state, H_3L^{N3O2} adopts a twisted conformation

DOI: 10.1021/acs.inorgchem.5b01380
Inorg. Chem. XXXX, XXX, XXX−XXX

featuring hydrogen bonds between phenol donors and imine acceptors (Figure 2).

The bimetallic complexes **1**−**6** were prepared by the reaction of H_3L^{N3O2} with 2 equiv of the appropriate MX_2 salt (M = Co, Cu, Zn; X = OTf, ClO_4) in the presence of NEt_3, along with addition of 2 equiv of the desired auxiliary ligand (1MeBI, bpy^{R2}, or S-^{iPr}OxPy). The resulting complexes are soluble in CH_2Cl_2 and polar aprotic solvents but insoluble in MeOH. All of the complexes possess a dark orange-brown color due to an absorption manifold with λ_{max} near 420 nm ($\varepsilon \approx 10^4$ M^{-1} cm^{-1}). This feature is attributed to π−π^* transitions of the L^{N3O2} ligand based on its intensity and consistent presence irrespective of metal ion or auxiliary ligand. As expected, dicopper complexes **1** and **2** give rise to ^{1}H NMR spectra with broad, paramagnetically shifted peaks (Figure S2). Using the Evans method, effective magnetic moments (μ_{eff}) of 2.38 ± 0.03 μ_B were measured for **1** and **2** at room temperature; these values are slightly less than the spin-only value of 2.56 μ_B expected for a binuclear species with two uncoupled S = 1/2 spins. In contrast, ^{1}H NMR spectra of the dizinc and dicobalt complexes (**3**−**5**) display sharp peaks with chemical shifts indicative of diamagnetic ground states (Figure S3). The lack of paramagnetism in the dicobalt complexes **4** and **5** is somewhat surprising, and it suggests the presence of strong antiferromagnetic coupling between the Co^{2+} centers—a matter that will be examined below.

3.B. Solid-State Structures of Complexes 1−5. Dark orange-brown crystals of the bimetallic complexes **1**−**5** suitable for X-ray diffraction analysis were grown from concentrated 1:1 solutions of CH_2Cl_2 and MeOH (or 1:1 acetone:MeOH in the case of **4**). Attempts to generate X-ray-quality crystals of **6** were unsuccessful. Selected bond lengths and angles are provided in Tables 1 and 2, and the representative structures of $[Cu_2(L^{N3O2})(1MeBI)_2]^+$ ($\mathbf{1}^+$) and $[Cu_2(L^{N3O2})(bpy)_2]^+$ ($\mathbf{2}^+$) are shown in Figure 3. In each structure, the L^{N3O2} ligand supports a bimetallic core in which the metal centers are solely bridged by the central diarylamido group. For example, the unit cell of **1** contains two symmetrically independent dicopper complexes with Cu1···Cu2 separations (d_{Cu-Cu}) of 3.0069(4) and 3.1202(4) (Table 1). The central $[Cu_2N]^{3+}$ unit exhibits a Cu1−N3−Cu2 angle near 97°, giving rise to an intermetallic "cleft". As intended, the L^{N3O2} framework provides meridional $[N,N,O]^{2-}$ coordination to both Cu^{2+} centers. The amido and phenolate donors of the fused pincer-type sites are pulled back slightly with O(1/2)−Cu(1/2)−N3 bond angles of 165 ± 3°. The Cu−O/N bond distances range from approximately 1.90 Å for the phenolate donors (O1,O2) to 2.05 Å for the bridging amido (N3) ligand. The additional coordination of two 1MeBI auxiliary ligands to each Cu^{2+} ion results in distorted square-planar geometries, although Cu1 is also weakly bound to a MeOH solvate (the Cu1−O6 distance is greater than 2.40 Å). The planes of the 1MeBI ligands are oriented nearly perpendicular to the square-planar $[CuN_3O]$ units, and the 1MeBI phenyl rings are positioned parallel to the imine groups on the inside of the cleft (Figure 3a).

The meridional binding mode of the L^{N3O2} framework causes each half of the ligand to adopt an orientation in which the salicyaldimine unit is roughly coplanar with the adjacent arylamido ring. However, these planar halves of the L^{N3O2} ligand are rotated relative to one another due to the twisting of the diarylamido unit. The solid-state structures of **1**−**5** revealed "twist angles" between 60° and 73° for the aryl rings bonded to N3 (Tables 1 and 2). Therefore, the bimetallic complexes possess idealized C_2 symmetry and exist as racemic mixtures of (*M*)- and (*P*)-enantiomers, as illustrated in Figure 4 [*Note*: The (*P*)-enantiomers of **1** and **2** are displayed in Figure 3]. In the next section, we will demonstrate that use of a chiral auxiliary ligand can force the L^{N3O2} ligand to favor one conformation over the other, resulting in a single diastereomeric product.

Table 1. Selected Bond Distances (Angstroms) and Angles (degrees) for the Two Symmetry-Independent Units (A and B) in the Crystal Structure of $[Cu_2(L^{N3O2})(1MeBI)_2]OTf$ (1)

bond lengths	A	B
Cu1···Cu2	3.0069(4)	3.1202(4)
Cu1−O1	1.908(2)	1.921(2)
Cu1−N1	1.940(2)	1.950(2)
Cu1−N3	2.049(2)	2.061(2)
Cu1−N4 (1MeBI)	1.991(2)	2.006(2)
Cu1−O6 (MeOH)	2.537(2)	2.404(2)
Cu2−O2	1.902(2)	1.898(2)
Cu2−N2	1.920(2)	1.925(2)
Cu2−N3	2.035(2)	2.039(2)
Cu2−N6 (1MeBI)	1.987(2)	1.982(2)
bond angles	**A**	**B**
Cu1−N3−Cu2	94.83(8)	99.10(8)
O1−Cu1−N1	92.55(7)	92.46(7)
O1−Cu1−N3	162.50(7)	162.62(7)
O1−Cu1−N4	88.53(7)	90.19(7)
N1−Cu1−N3	84.05(7)	84.20(7)
N1−Cu1−N4	175.12(8)	175.51(8)
N3−Cu1−N4	96.31(7)	94.32(7)
O2−Cu2−N2	94.05(7)	93.55(7)
O2−Cu2−N3	164.17(7)	167.41(7)
O2−Cu2−N6	89.15(7)	89.46(8)
N2−Cu2−N3	84.13(7)	84.46(7)
N2−Cu2−N6	166.02(8)	168.43(8)
N3−Cu2−N6	96.40(7)	94.96(8)
twist angle[a]	66.3	73.2

[a]The twist angle refers to the angle between the planes of the aryl rings of the central amido unit.

The three bpy-containing complexes **2**−**4** (Chart 1) yield quasi-isomorphous crystals in the monoclinic $P2_1/c$ space group (Table S1). The structure of $[Cu_2(L^{N3O2})(bpy)_2]^+$ ($\mathbf{2}^+$), shown in Figure 3b, is representative of the series. In each complex, the two metal ions occupy equivalent binding sites defined by the pincer-type *N,N,O*-chelates of the L^{N3O2} ligand, which adopts the same C_2-symmetric ("twisted") conformation described above. Coordination of the bidentate bpy ligands results in five-coordinate M^{2+} ions with distorted square-pyramidal (**4**) or trigonal-bipyramidal (**3**) geometries, as indicated by τ values[37] in Table 2. The presence of the fifth donor causes the M^{2+} ions to move out of the plane defined by the meridional L^{N3O2} chelate by amounts ranging from 0.36 (**4**) to 0.80 Å (**3**). Each bpy ligand places one pyridyl donor trans to the imine N atom (N1 or N2), while the other is located outside the cleft in a position opposite the intermetallic bond vector. Unlike the 1MeBI ligands in **1**, the bpy ligands in **2**−**4** do not block access to the space between the metal ions, thus permitting the binding of small molecules like O_2 (vide infra).

Table 2 reveals several trends in metric parameters across the **2**−**4** series. The $M-L_{N/O}$ bond distances and intermetallic separations are strongly dependent on metal ion identity, both following the general order of Zn > Cu > Co. Of particular note is the observed Co···Co distance (d_{Co-Co}) of 2.701 Å, which is

DOI: 10.1021/acs.inorgchem.5b01380
Inorg. Chem. XXXX, XXX, XXX−XXX

Table 2. Selected Bond Distances (Angstroms) and Angles (degrees) Obtained from the Crystal Structures of Complexes 2−4

	complex 2		complex 3		complex 4	
bond distances	Cu1	Cu2	Zn1	Zn2	Co1	Co2
M1···M2	2.9667(5)		3.2820(5)		2.7010(5)	
M1−O1/M2−O2	1.924(2)	1.921(2)	1.952(1)	1.956(1)	1.899(2)	1.895(2)
M1−N1/M2−N2	1.940(2)	1.940(2)	2.054(1)	2.058(1)	1.889(2)	1.888(2)
M1−N3/M2−N3	2.063(2)	2.052(2)	2.086(1)	2.103(1)	1.966(2)	1.964(2)
M1−N4/M2−N6 (bpy)	2.201(2)	2.228(2)	2.100(1)	2.100(1)	2.064(2)	2.059(2)
M1−N5/M2−N7 (bpy)	2.010(2)	2.008(2)	2.116(1)	2.118(1)	1.942(2)	1.943(2)
M−$L_{N/O}$ (ave)	2.028	2.030	2.062	2.067	1.952	1.950
	complex 2		complex 3		complex 4	
bond angles	Cu1	Cu2	Zn1	Zn2	Co1	Co2
M1−N3−M2	92.28(8)		103.15(6)		86.85(8)	
O1/O2−M−N1/N2	92.69(8)	92.58(9)	89.07(5)	88.52(5)	93.52(8)	93.92(7)
O1/O2−M−N3	146.38(8)	152.33(8)	140.53(5)	133.17(5)	158.41(7)	156.69(7)
O1/O2−M−N4/N6	114.49(8)	112.33(8)	114.66(5)	118.85(5)	106.01(7)	105.79(7)
O1/O2−M−N5/N7	91.23(8)	88.30(8)	90.43(5)	94.39(5)	84.38(7)	86.33(7)
N1/N2−M−N3	83.05(8)	84.09(9)	81.72(5)	80.43(5)	85.02(8)	84.76(7)
N1/N2−M−N4/N6	93.85(8)	94.33(8)	97.25(5)	97.34(5)	91.98(8)	91.57(8)
N1/N2−M−N5/N7	171.34(9)	171.63(9)	174.87(5)	175.18(5)	171.85(8)	172.13(8)
N3−M−N4/N6	99.09(8)	95.33(8)	104.57(5)	107.69(5)	95.57(8)	97.51(8)
N3−M−N5/N7	97.87(8)	98.93(8)	101.83(5)	100.25(5)	99.83(8)	98.11(7)
N4/N6−M−N5/N7	77.50(8)	77.66(8)	78.33(5)	77.89(5)	81.08(8)	80.81(8)
τ value[a]	0.42	0.32	0.57	0.70	0.22	0.26
twist angle[b]	64.0		67.6		61.7	

[a]For definition of the τ value, see ref 37. [b]The twist angle refers to the angle between the planes of the aryl rings of the central amido unit.

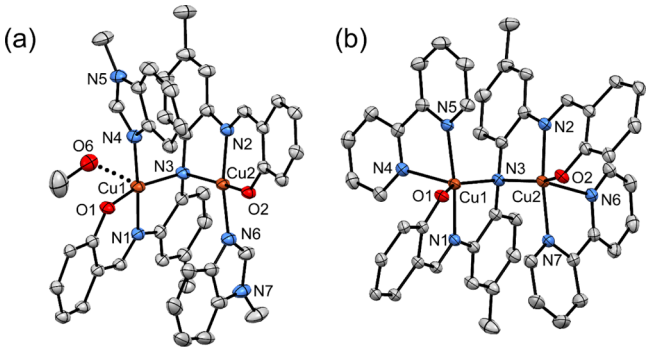

Figure 3. Thermal ellipsoid plots (40% probability) derived from the X-ray crystal structures of complexes 1 (a) and 2 (b). Hydrogen atoms, counteranions, and *tert*-butyl substituents of the phenolate donors have been omitted for the sake of clarity.

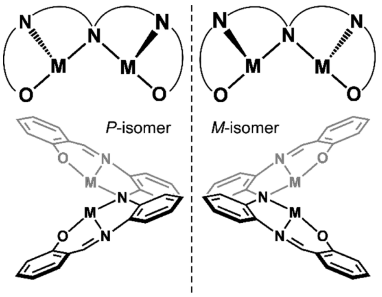

Figure 4. Illustration of the two possible orientations of the C_2-symmetric L^{N3O2} ligand in complexes 1−6. The designations of the atropisomers (*M* and *P*) were based on rules developed for binaphthyl systems.

remarkably short given the presence of only one bridging ligand. A search of the Cambridge Structural Database found that nearly all di- and polycobalt complexes with d_{Co-Co} < 2.8 Å possess multiple bridging groups. While it is not proper to invoke the existence of a Co−Co bond in 4, since the intermetallic distance exceeds the sum of van der Waals radius of Co (2.486 Å), this feature points to strong electronic interactions between the Co^{2+} centers. In addition, the average Co−$L_{N/O}$ distance of 1.951 Å in 4 is unusually small. High-spin Co^{2+} complexes with N_4O ligand sets typically exhibit average Co−$L_{N/O}$ lengths of 2.07 ± 0.05 Å, while the handful of low-spin [CoN_4O] structures in the literature feature average Co−$L_{N/O}$ bonds of 1.95 ± 0.05 Å.[38] Thus, the crystallographic data indicate that 4 consists of two low-spin Co^{2+} centers in square-pyramidal environments. The electronic structure of this complex is described in more detail in the DFT section below.

Not surprisingly, the solid-state structures of complex 4 and its bpy^{Br2}-containing congener (5) are quite similar, with one exception: the addition of bromine substituents causes a modest lengthening of the Co···Co distance from 2.701 to 2.837 Å, with a concomitant increase in the Co1−N3−Co2 bond angle (Table S2). Otherwise, the Co−N/O bond lengths in 4 and 5 differ by less than 0.025 Å, indicating that both complexes feature low-spin Co^{2+} centers.

3.C. Formation of the Chiral Complex [Zn_2(*P*-L^{N3O2})-(*S*-^{iPr}OxPy)$_2$]OTf (6). There has been a long-standing interest in developing chiral bimetallic complexes for use in asymmetric catalysis and supramolecular chemistry.[39] As noted above, the bimetallic complexes 1−5 possess helical chirality due to the C_2 symmetry imposed by the L^{N3O2} framework (Figure 4). We were curious whether the use of a chiral auxiliary ligand would bias the helical sense of the L^{N3O2} ligand, thereby yielding a single diastereomeric product. To this end, the reaction of $Zn(OTf)_2$ and H_3L^{N2O3} with the auxiliary ligand *S*-^{iPr}OxPy (Chart 1) was performed in the presence of base. The ^{1}H NMR spectrum of the resulting product (6), shown in Figure 5,

DOI: 10.1021/acs.inorgchem.5b01380
Inorg. Chem. XXXX, XXX, XXX−XXX

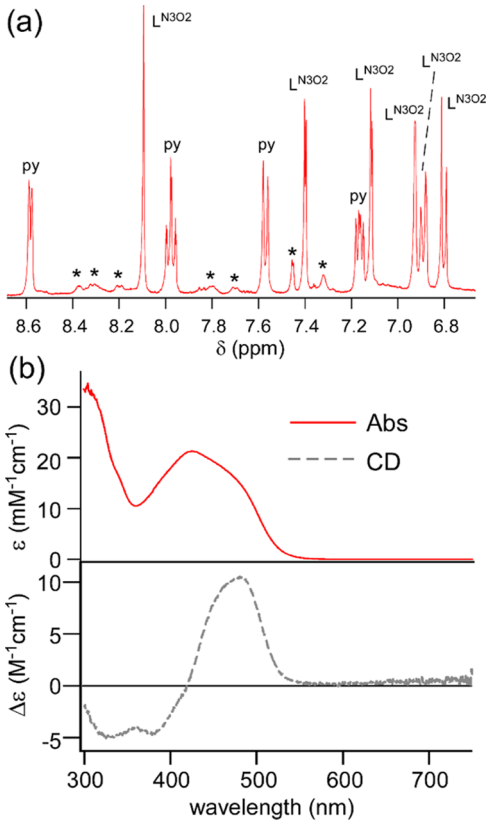

Figure 5. (Top) Aromatic region of the ^{1}H NMR spectrum of complex **6** in MeCN-d_3. Peaks are assigned to either the pyridyl (py) moiety of *S*-^{iPr}OxPy or the $\mathbf{L}^{N3O2}$ ligand based on splitting patterns and comparison to data collected for $H_3\mathbf{L}^{N3O2}$ and **3**. Each of the 10 assigned features integrates to two H atoms. Ill-defined peaks marked with asterisks arise from the minor diastereomeric product. (Bottom) Absorption and CD spectra of **6** collected at room temperature in MeCN.

displays only one set of well-resolved peaks arising from the $\mathbf{L}^{N3O2}$ and *S*-^{iPr}OxPy ligands, indicating that the material largely consists of a single diastereomer. However, a number of weak and poorly resolved features are also apparent (indicated by the asterisks in Figure 5a); if these are assigned to the minor diastereomer then relative peak heights suggest that at least 85% of **6** exists as the major product. Further evidence of diastereomeric excess is provided by circular dichroism (CD) spectroscopy. As shown in Figure 5b, the CD spectrum of **6** exhibits positive and negative bands at 470 and 380 nm, respectively, corresponding to the two overlapping bands in the absorption spectrum. Since these features arise from $\mathbf{L}^{N3O2}$-based transitions (vide supra), we can conclude that the $\mathbf{L}^{N3O2}$ ligand largely exists in a single helical conformation. As expected, the CD spectrum of the bpy-containing dizinc(II) analog (**3**) is featureless across the UV−vis region (Figure S4) because the complex exists as a racemic mixture of *M*- and *P*-enantiomers.

In complex **6**, the oxazoline ring of the asymmetric *S*-^{iPr}OxPy ligand can be positioned either cis or trans to the imine donors (N1 and N2). The combination of geometric and stereoisomerism gives rise to four possible C_2-symmetric structures: *trans*-(*M*,*S*,*S*), *cis*-(*M*,*S*,*S*), *trans*-(*P*,*S*,*S*), and *cis*-(*P*,*S*,*S*). The energy of each isomer was computed using DFT, and the most stable structure was found to be *cis*-(*P*,*S*,*S*), shown in Figure 6. This isomer minimizes steric interactions between the isopropyl

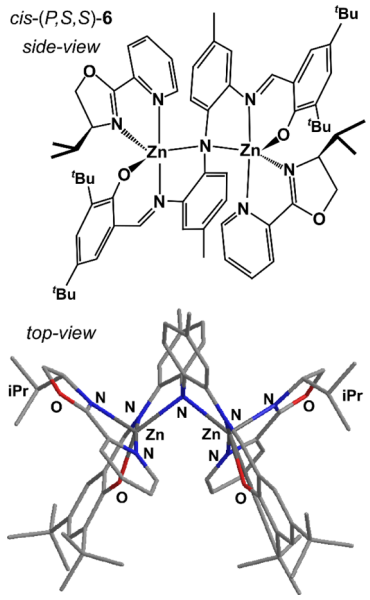

Figure 6. Depictions of the *cis*-(*P*,*S*,*S*) diastereomer of complex **6**.

groups of *S*-^{iPr}OxPy and the $\mathbf{L}^{N3O2}$ ligand. Relative to *cis*-(*P*,*S*,*S*), the *cis*-(*M*,*S*,*S*) diastereomer is higher in energy by 6.4 kcal/mol because the isopropyl groups are directed toward the central aryl rings. The *trans*-(*M*,*S*,*S*) and *trans*-(*P*,*S*,*S*) structures are even more unfavorable energetically (7.0 and 9.9 kcal/mol, respectively), as the isopropyl groups sterically clash with either the phenyl rings of the diarylamido unit (*M*-isomer) or the *tert*-butyl substituents of the phenolate donors (*P*-isomer). These DFT results suggest that the major isomer of **6**, observed spectroscopically in solution, corresponds to the *cis*-(*P*,*S*,*S*) diasteromer. On the basis of the computed energy differences, we would not expect to detect the minor isomer at room temperature. The fact that the minor *cis*-(*M*,*S*,*S*) diastereomer is observed in the ^{1}H NMR spectrum of **6** (Figure 5) suggests that the *M*- and *P*-isomers cannot easily interconvert to yield the thermodynamically favored product, and thus, the product ratio is also affected by kinetic factors.

3.D. Electrochemical Studies. Voltammetric methods were used to examine the electrochemical properties of complexes **2**−**5** in MeCN solutions with 0.1 M $(NBu_4)PF_6$ as the supporting electrolyte and scan rates of 100 mV/s. The reported potentials are relative to the Fc/Fc^+ couple. The cyclic and square-wave voltammograms (CV and SWV) of the dicopper complex **2**, shown in Figure 7, reveal three redox features at negative potentials of −1.40, −1.83, and −2.06 V. The two lowest potential events are quasi-reversible, whereas the peak at −1.40 V is irreversible. The SWV of the analogous dicobalt complex (**4**) displays three peaks at very similar potentials of −1.42, −1.81, and −2.04 V. Assignment of these features to either metal- or ligand-based reductions is aided by comparison with data collected for **3**, which contains redox-inactive Zn^{2+} ions. The voltammogram of **3** retains the two lowest potential features at −1.95 and −2.08 V; however, the first reduction wave is absent (Figure 7). Therefore, we can confidently assign the two events at $E < -1.7$ V to reduction of the bpy auxiliary ligands, while the event near −1.4 V is attributed to reduction of the Cu_2^{4+} and Co_2^{4+} units to yield mixed-valent species. Electrochemical data obtained for the bpy^{Br2}-containing dicobalt complex (**5**) provide further confirmation of these assignments. Relative to **4**, the two

DOI: 10.1021/acs.inorgchem.5b01380
Inorg. Chem. XXXX, XXX, XXX−XXX

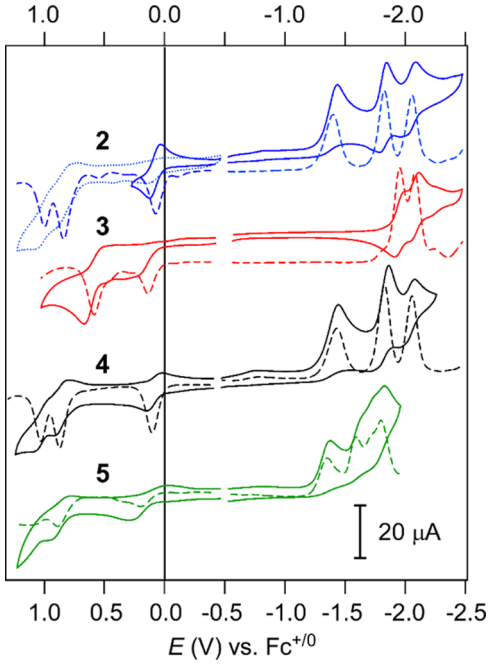

Figure 7. Cyclic voltammograms (solid lines) of complexes **2**–**5** collected in MeCN with 0.1 M $(NBu_4)PF_6$ as the supporting electrolyte. Corresponding square-wave voltammograms are indicated by the dashed lines. All scan rates were 100 mV/s. Data in the high- and low-potential regions were generally collected in separate scans. Two CVs with different sweep widths are provided for complex **2**.

lowest potentials peaks of **5** are shifted positively by ∼0.23 V, reflecting the electron-withdrawing capacity of the 4-Br substituents. In contrast, the metal-based peak experiences a much smaller shift from −1.42 to −1.33 V. The redox-active nature of bpy ligands has been well-established in numerous studies,[40] including recent efforts by the Wieghardt group.[41,42] The homoleptic $[Fe(bpy)_3]^{2+}$ complex, for example, exhibits sequential reductions of the three bpy ligands at potentials of −1.66, −1.94, and −2.10 V.[41] The corresponding potentials in **2**–**4** are more negative than those reported for $[Fe(bpy)_3]^n$ by 100–150 mV, likely due to the trianionic nature of the $\mathbf{L^{N3O2}}$ framework.

To more positive potentials, all four complexes exhibit a feature between 0.07 and 0.19 V. While this redox event is quasi-reversible for **2** and **4** (ΔE = 83 and 115 mV, respectively), it is irreversible in the cases of **3** and **5**, as evident in the diminished intensity of the corresponding peaks in the SWV (Figure 7). Given its presence across the **2**–**5** series, it is logical to attribute this feature to a ligand-based event. Indeed, a survey of the literature revealed that the diarylamido moieties of PNP pincer ligands are oxidized between +0.32 and −0.34 V,[18,21b,43] and the di(2-pyrazolylaryl)amido pincers of Gardinier and co-workers undergo oxidation near 0.0 V.[6e,44] The common feature near 0.1 V in complexes **2**–**5** is therefore assigned to oxidation of the μ-NAr_2 unit of the $\mathbf{L^{N3O2}}$ ligand. Evidence for formation of a ligand-based radical upon one-electron oxidation of **4** is provided in the EPR and DFT studies described in section 3.E.

In addition, complexes **2** and **4** exhibit two closely spaced waves centered near 0.90 V (Figure 7). These features correspond to successive oxidations of the divalent metal ions, although the processes likely involve partial oxidation of the phenolate donors as well. Support for the latter conclusion is found in the CV and SWV data of the dizinc(II) analog (**3**), which display an ill-defined event in the same region despite the absence of redox-active metal ions. Previous studies of related mononuclear complexes have detected phenolate oxidations in the range of 0.5–1.5 V versus $Fc^{+/0}$,[45] although it is often difficult to distinguish between ligand- and metal-based events due to the high covalency of metal–phenolate bonds.

3.E. Spectroscopic and Computational Studies of 4 and 4^{ox}. Density functional theory (DFT) was employed to examine the unusual electronic properties of $[Co_2(\mathbf{L^{N3O2}})(bpy)_2]^+$ ($\mathbf{4^+}$), namely, its diamagnetism and short Co–Co distance. These calculations employed the hybrid B3LYP functional and crystallographically determined structure, although the *tert*-butyl substituents of the phenolate rings were replaced with H atoms. The proper wave function for the S = 0 ground state was obtained using the broken-symmetry (BS-DFT) approach pioneered by Noodleman and others.[46] The BS-DFT calculations revealed strong antiferromagnetic (AF) coupling between the low-spin Co^{2+} centers, with a computed exchange coupling constant (J) of −1050 cm^{-1} (based on the Yamaguchi definition[47] of $H = -2JS_A \cdot S_B$). The AF coupling arises from direct overlap of the $3d(z^2)$-based singly occupied molecular orbitals (SOMOs) localized on each Co^{2+} center (the local z axes are directed along the axial Co–N bonds; see Figure S5). The overlap integral (S) for these two magnetic orbitals with opposite spin is 0.29, consistent with the presence of a *partial* Co–Co bond in **4**. The magnitude of the computed J value ensures that the triplet state is not accessible at room temperature.

On the basis of the electrochemical results presented above, we sought to generate the oxidized form of complex **4** via chemical means. Treatment of **4** with 1 equiv of 1′-acetylferrocenium (AcFc; E = 0.27 V) in MeCN causes the ligand-based absorption band near 400 nm to red shift and decrease in intensity (Figure 8; inset), indicative of a change in the π system of the $\mathbf{L^{N3O2}}$ ligand. The X-band EPR spectrum of the one-electron-oxidized species ($\mathbf{4^{ox}}$), shown in Figure 8, consists of a broad derivative feature centered at g = 2.02. The presence of ^{59}Co hyperfine splitting at both high and low fields is particularly evident in the second-harmonic spectrum. The data is nicely simulated (Figure 8) with the following spin-Hamiltonian parameters: a pseudoaxial **g** tensor ($g_{x,y,z}$ = 2.059, 2.037, 1.995) and hyperfine coupling constants of $A_{x,y,z}$ = 23, 21 and 7.1 G for both Co ions. Low-spin, five-coordinate Co^{2+} centers typically display A_{max} values between 80 and 120 G and g_x values near 2.40.[48] In contrast, the modest g anisotropy and small A values of $\mathbf{4^{ox}}$ more closely resemble the EPR parameters of mononuclear Co/O_2 adducts ($g_{x,y}$ = 2.08 and $A_{max} \approx$ 20 G), where the unpaired spin largely resides on the superoxo ligand.[48] Therefore, the EPR data provide further evidence that one-electron oxidation of **4** generates a ligand-based radical, although the unpaired spin is partially delocalized over the two Co ions.

The nature of the $\mathbf{L^{N3O2}}$-based radical was probed with BS-DFT calculations. Because a crystal structure of $\mathbf{4^{ox}}$ is not available, a computational model was obtained via geometry optimization. Comparison of Mulliken spin populations indicate that one-electron oxidation of **4** to $\mathbf{4^{ox}}$ causes a dramatic increase in the amount of unpaired spin density on the $\mathbf{L^{N3O2}}$ ligand (from 0.04 to 0.74 spins), while the spin of the Co centers remains nearly constant. The $\mathbf{4^{ox}}$ model contains three unpaired electrons: two are localized in $Co(dz^2)$-based MOs, while the third is primarily localized on the central μ-NAr_2 unit

DOI: 10.1021/acs.inorgchem.5b01380
Inorg. Chem. XXXX, XXX, XXX–XXX

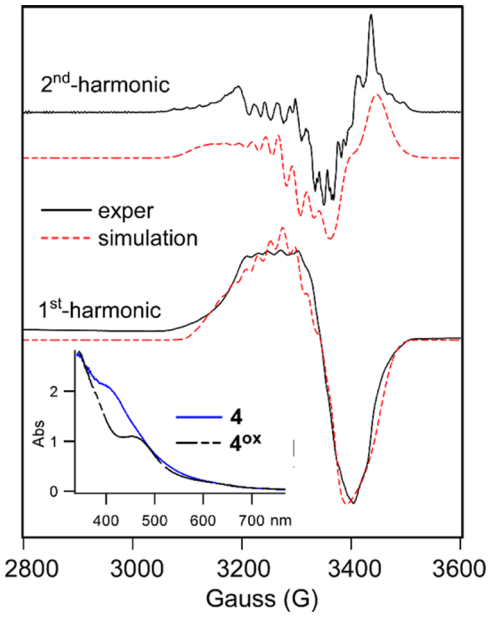

Figure 8. X-band EPR spectrum of $\mathbf{4^{ox}}$ (black, solid) in frozen MeCN at 77 K. The presence of ^{59}Co hyperfine splitting is clearly apparent in the corresponding second-harmonic data (top). Simulated spectra (red, dashed) were obtained with the following parameters: $g_{x,y,z}$ = 2.059, 2.037, 1.995; $A_{x,y,z}$ = 23, 21, and 7.1 G; mwFreq = 9.434 GHz. (Inset) Absorption spectra of **4** (blue, solid) and $\mathbf{4^{ox}}$ (black, dashed) in MeCN (conc. = 0.1 mM).

of the $\mathbf{L^{N3O2}}$ ligand. The contour plot of the $\mathbf{L^{N3O2}}$-based SOMO, shown in Figure S6, reveals overlap between the $2p_z$ orbital of the bridging N atom (N3) and Co 3d orbitals, accounting for the observable ^{59}Co hyperfine splitting in the EPR spectrum of $\mathbf{4^{ox}}$. The DFT calculations are therefore consistent with the formulation of $\mathbf{4^{ox}}$ as $[Co^{2+}_2(\mathbf{L^{N3O2,\bullet}})(bpy)_2]^{2+}$, in agreement with the electrochemical and spectroscopic data already presented.

3.F. Reactivity of Complex 5 with O_2. If exposed to air, solutions of **5** in 1:1 CH_2Cl_2:MeOH provide dark-brown crystals with unit cell parameters distinct from those determined for anaerobically grown crystals (Table S1). X-ray diffraction analysis determined that the aerobic crystals consist of $[Co_2(O_2)(\mathbf{L^{N3O2}})(bpy)_2]ClO_4$ ($\mathbf{5\text{-}O_2}$), where a diatomic O_2 ligand bridges in a μ-1,2-fashion between the six-coordinate cobalt centers (Figure 9). The O3−O4 distance of 1.372(6) Å identifies the bridging ligand as a peroxide (O_2^{2-}) moiety. The $[Co_2O_2]$ unit adopts a twisted orientation with a Co−O−O−Co dihedral angle of 56.3° and Co1···Co2 distance of 3.253(1) Å—considerably longer than the d_{Co-Co} value of 2.70 Å found for **5**. Significantly, the $\mathbf{5\text{-}O_2}$ structure proves that small molecules are able to access the open coordination sites within the intermetallic cleft, despite the steric bulk of the nearby *tert*-butyl substituents of the phenolate donors. Moreover, the dramatic 0.55 Å increase in intermetallic separation upon O_2 binding highlights the structural pliability of the $\mathbf{L^{N3O2}}$ scaffold.

Comparison of metric parameters indicates that the conversion of $\mathbf{5 \rightarrow 5\text{-}O_2}$ involves oxidation of the low-spin Co^{2+} centers to Co^{3+}. This conclusion is evident in the shortening of the axial Co1−N4 and Co2−N6 bonds by ∼0.09 Å due to the transfer of two Co(dz^2)-based electrons to O_2 (Table S2). In contrast, O_2 binding does not cause significant changes in the O−C, N−C, and C−C bond lengths of the $\mathbf{L^{N3O2}}$ ligand, indicating a lack of radical character. On the basis

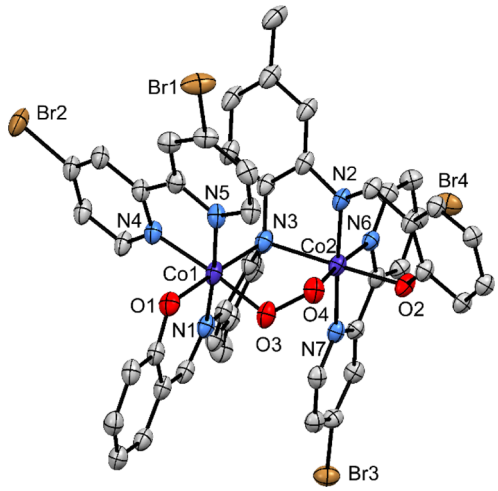

Figure 9. Thermal ellipsoid plot (30% probability) derived from the X-ray crystal structure of complex $\mathbf{5\text{-}O_2}$. Hydrogen atoms, counter-anions, and *tert*-butyl substituents of the phenolate donors have been omitted for the sake of clarity.

of the electrochemical data presented above, one might have assumed that O_2 binding would result in oxidation of the $\mathbf{L^{N3O2}}$ ligand. It appears that the increase in coordination number from 5 to 6, coupled with the dianionic nature of the peroxide ligand, suppresses the redox potentials of the Co centers relative to $\mathbf{L^{N3O2}}$. These factors favor metal-centered oxidation over ligand-based oxidation in formation of the dicobalt-peroxo complex.

4. CONCLUSIONS

As demonstrated in this manuscript, the easily prepared $\mathbf{L^{N3O2}}$ ligand is capable of supporting homobimetallic frameworks (M = Co, Cu, Zn) with adjacent pincer-type compartments consisting of a bridging diarylamido group and salicyaldimine chelates (Figure 1). The "fused" nature of the pincer sites results in short intermetallic distances between 2.7 and 3.3 Å, as determined by X-ray crystallography. While several complexes with $[M_2(\mu\text{-}NAr_2)_2]$ cores have been reported in the literature, complexes **1**−**6** are rather unique in containing only a single diarylamido bridge.[49] Because of this, the unsaturated metal centers are capable of binding auxiliary ligands, such as 1MeBI, bpy^{R2}, and $S\text{-}^{iPr}$OxPy. These auxiliary ligands impart additional features to the bimetallic complexes that may prove useful in future applications; for example, the noninnocent bpy^{R2} ligands in **2**−**5** account for two redox events at low potentials, while the optically active $S\text{-}^{iPr}$OxPy ligand compels the C_2-symmetric structures to favor the *P*-configuration. Thus, the $\mathbf{L^{N3O2}}$ ligand provides a versatile platform for the synthesis of bimetallic complexes with tunable electronic and structural properties.

Electrochemical studies of the bpy-containing complexes **2** and **4** found six redox couples over a range of 3.0 V arising from both metal- and ligand-based events. The one-electron oxidation of **4** near 0.1 V triggers formation of a $\mathbf{L^{N3O2}}$-based radical localized on the diarylamido donor, as indicated by EPR and DFT studies of $\mathbf{4^{ox}}$. This finding is consistent with previous studies of $[M_2(\mu\text{-}NAr_2)_2]$ complexes. The ability to perform several electron transfers is critical for synthetic catalysts involved in small-molecule activation, such as the reduction of O_2 (to H_2O) and H^+ (to H_2). Redox-active ligands, like bpy and $\mathbf{L^{N3O2}}$ in complexes **2**−**5**, can serve as electron reservoirs for multielectron transformations. Most significantly, *the*

DOI: 10.1021/acs.inorgchem.5b01380
Inorg. Chem. XXXX, XXX, XXX−XXX

complexes described here feature open and accessible coordination sites between the metal centers for small-molecule binding. As highlighted by formation of the μ-peroxo complex **5-O$_2$** (Figure 9), the $\mathbf{L}^{N3O2}$ scaffold has the structural flexibility to accommodate the changes in coordination number and oxidation state that occur during catalytic cycles. Therefore, we are currently evaluating the ability of these promising binuclear complexes to serve as electrocatalyts for the reduction of O_2 and H^+.

■ ASSOCIATED CONTENT

Supporting Information

The Supporting Information is available free of charge on the ACS Publications website at DOI: 10.1021/acs.inorgchem.5b01380.

^{1}H NMR spectra of complexes **1**−**5**, absorption and CD spectra of **3**, metric parameters for **5** and **5-O$_2$**, and contour plot of the singly occupied molecular orbital (SOMO) of **4^{ox}** (PDF)

Crystallographic data in CIF format (CIF)

■ AUTHOR INFORMATION

Corresponding Author

*E-mail: adam.fiedler@marquette.edu. Fax: 414-288-7066.

Notes

The authors declare no competing financial interest.

■ ACKNOWLEDGMENTS

This research was generously supported by Marquette University and the U.S. National Science Foundation (NSF) (CHE-1056845). We thank Dr. Thomas Brunold for allowing us to collect CD spectra in his laboratory and Dr. James R. Gardiner for helpful discussions.

■ REFERENCES

(1) (a) *The Chemistry of Pincer Compounds*; Morales-Morales, D., Jensen, C. M., Eds.; Elsevier: Amsterdam, 2007. (b) *The Pincer Ligand: Its Chemistry and Applications (Catalytic Science)*; Chase, P. A., Koten, G. v., Eds.; Imperial College Press: London, 2010. (c) O'Reilly, M. E.; Veige, A. S. *Chem. Soc. Rev.* **2014**, *43*, 6325−6369.

(2) (a) van Koten, G. *J. Organomet. Chem.* **2013**, *730*, 156−164. (b) Szabo, K. J. *Top. Organomet. Chem.* **2013**, *40*, 203−242. (c) Albrecht, M.; Lindner, M. M. *Dalton Trans.* **2011**, *40*, 8733−8744. (d) van der Boom, M. E.; Milstein, D. *Chem. Rev.* **2003**, *103*, 1759−1792.

(3) (a) Wieczorek, B.; Dijkstra, H. P.; Egmond, M. R.; Gebbink, R. J. M. K.; van Koten, G. *J. Organomet. Chem.* **2009**, *694*, 812−822. (b) Albrecht, M.; van Koten, G. *Angew. Chem., Int. Ed.* **2001**, *40*, 3750−3781.

(4) (a) Hawk, J. L.; Craig, S. L. *Top. Organomet. Chem.* **2013**, *40*, 319−352. (b) South, C. R.; Weck, M. *Langmuir* **2008**, *24*, 7506−7511.

(5) (a) Fan, L.; Foxman, B. M.; Ozerov, O. V. *Organometallics* **2004**, *23*, 326−328. (b) Liang, L.-C. *Coord. Chem. Rev.* **2006**, *250*, 1152−1177. (c) Mindiola, D. J. *Acc. Chem. Res.* **2006**, *39*, 813−821.

(6) (a) Kieltsch, I.; Dubinina, G. G.; Hamacher, C.; Kaiser, A.; Torres-Nieto, J.; Hutchison, J. M.; Klein, A.; Budnikova, Y.; Vicic, D. A. *Organometallics* **2010**, *29*, 1451−1456. (b) Inagaki, T.; Phong, L. T.; Furuta, A.; Ito, J.-i.; Nishiyama, H. *Chem. - Eur. J.* **2010**, *16*, 3090−3096. (c) Peters, J. C.; Harkins, S. B.; Brown, S. D.; Day, M. W. *Inorg. Chem.* **2001**, *40*, 5083−5091. (d) Breitenfeld, J.; Vechorkin, O.; Corminboeuf, C.; Scopelliti, R.; Hu, X. *Organometallics* **2010**, *29*, 3686−3689. (e) Wanniarachchi, S.; Liddle, B. J.; Toussaint, J.; Lindeman, S. V.; Bennett, B.; Gardinier, J. R. *Dalton Trans.* **2010**, *39*, 3167−3169. (f) Hollas, A. M.; Gu, W.; Bhuvanesh, N.; Ozerov, O. V. *Inorg. Chem.* **2011**, *50*, 3673−3679. (g) Mudadu, M. S.; Singh, A. N.; Thummel, R. P. *J. Org. Chem.* **2008**, *73*, 6513−6520. (h) Gaunt, J. A.; Gibson, V. C.; Haynes, A.; Spitzmesser, S. K.; White, A. J. P.; Williams, D. J. *Organometallics* **2004**, *23*, 1015−1023. (i) Barbe, J.-M.; Habermeyer, B.; Khoury, T.; Gros, C. P.; Richard, P.; Chen, P.; Kadish, K. M. *Inorg. Chem.* **2010**, *49*, 8929−8940.

(7) Fafard, C. M.; Adhikari, D.; Foxman, B. M.; Mindiola, D. J.; Ozerov, O. V. *J. Am. Chem. Soc.* **2007**, *129*, 10318−10319.

(8) Golisz, S. R.; Labinger, J. A.; Bercaw, J. E. *Organometallics* **2010**, *29*, 5026−5032.

(9) (a) Zarkesh, R. A.; Heyduk, A. F. *Organometallics* **2011**, *30*, 4890−4898. (b) Broere, D. L. J.; Demeshko, S.; de Bruin, B.; Pidko, E. A.; Reek, J. N. H.; Siegler, M. A.; Lutz, M.; van der Vlugt, J. I. *Chem. - Eur. J.* **2015**, *21*, 5879−5886.

(10) Chan, C.-W.; Mingos, M. P.; White, A. J. P.; Williams, D. J. *Chem. Commun.* **1996**, 81−83.

(11) (a) Steenwinkel, P.; Kooijman, H.; Smeets, W. J. J.; Spek, A. L.; Grove, D. M.; Van Koten, G. *Organometallics* **1998**, *17*, 5411−5426. (b) Zhao, C.-Q.; Jennings, M. C.; Puddephatt, R. J. *Dalton Trans.* **2008**, 1243−1250.

(12) Kocher, S.; van Klink, G. P. M.; van Koten, G.; Lang, H. *J. Organomet. Chem.* **2003**, *684*, 230−234.

(13) Tsubomura, T.; Tanihata, T.; Yamakawa, T.; Ohmi, R.; Tamane, T.; Higuchi, A.; Katoh, A.; Sakai, K. *Organometallics* **2001**, *20*, 3833−3835.

(14) Herbert, D. E.; Ozerov, O. V. *Organometallics* **2011**, *30*, 6641−6654.

(15) Samanta, S.; Demesko, S.; Dechert, S.; Meyer, F. *Angew. Chem.* **2015**, *54*, 583−587.

(16) van der Vlugt, J. I.; Demeshko, S.; Dechert, S.; Meyer, F. *Inorg. Chem.* **2008**, *47*, 1576−1585.

(17) Harkins, S. B.; Peters, J. C. *J. Am. Chem. Soc.* **2005**, *127*, 2030−2031.

(18) Adhikari, D.; Mossin, S.; Basuli, F.; Dible, B. R.; Chipara, M.; Fan, H.; Huffman, J. C.; Meyer, K.; Mindiola, D. J. *Inorg. Chem.* **2008**, *47*, 10479−10490.

(19) Fout, A. R.; Basuli, F.; Fan, H.; Tomaszewski, J.; Huffman, J. C.; Baik, M.-H.; Mindiola, D. J. *Angew. Chem., Int. Ed.* **2006**, *45*, 3291−3295.

(20) (a) Harkins, S. B.; Mankad, N. P.; Miller, A. J. M.; Szilagyi, R. K.; Peters, J. C. *J. Am. Chem. Soc.* **2008**, *130*, 3478−3485. (b) Mankad, N. P.; Harkins, S. B.; Antholine, W. E.; Peters, J. C. *Inorg. Chem.* **2009**, *48*, 7026−7032.

(21) (a) Adhikari, D.; Mossin, S.; Basuli, F.; Huffman, J. C.; Szilagyi, R. K.; Meyer, K.; Mindiola, D. J. *J. Am. Chem. Soc.* **2008**, *130*, 3676−3682. (b) Radosevich, A. T.; Melnick, J. G.; Stoian, S. A.; Bacciu, D.; Chen, C.-H.; Foxman, B. M.; Ozerov, O. V.; Nocera, D. G. *Inorg. Chem.* **2009**, *48*, 9214−9221.

(22) (a) Suarez, A. I. O.; Lyaskovskyy, V.; Reek, J. N. H.; van der Vlugt, J. I.; de Bruin, B. *Angew. Chem., Int. Ed.* **2013**, *52*, 12510−12529. (b) Lyaskovskyy, V.; de Bruin, B. *ACS Catal.* **2012**, *2*, 270−279.

(23) Ma, L.; Woloszynek, R. A.; Chen, W.; Ren, T.; Protasiewicz, J. D. *Organometallics* **2006**, *25*, 3301−3304.

(24) (a) Wong, J. L.; Sanchez, R. H.; Logan, J. G.; Zarkesh, R. A.; Ziller, J. W.; Heyduk, A. F. *Chem. Sci.* **2013**, *4*, 1906−1910. (b) Sharma, S. K.; May, P. S.; Jones, M. B.; Lense, S.; Hardcastle, K. I.; MacBeth, C. E. *Chem. Commun.* **2011**, *47*, 1827−1829. (c) Min, K. S.; Weyhermueller, T.; Wieghardt, K. *Dalton Trans.* **2004**, 178−186. (d) Olmstead, M. M.; Power, P. P.; Shoner, S. C. *Inorg. Chem.* **1991**, *30*, 2547−2551.

(25) (a) Vigato, P. A.; Peruzzo, V.; Tamburini, S. *Coord. Chem. Rev.* **2012**, *256*, 953−1114. (b) Clarke, R. M.; Storr, T. *Dalton Trans.* **2014**, *43*, 9380−9391. (c) Radlauer, M. R.; Buckley, A. K.; Henling, L. M.; Agapie, T. *J. Am. Chem. Soc.* **2013**, *135*, 3784−3787. (d) Radlauer, M. R.; Day, M. W.; Agapie, T. *J. Am. Chem. Soc.* **2012**, *134*, 1478−1481.

(26) Stoll, S.; Schweiger, A. *J. Magn. Reson.* **2006**, *178*, 42−55.

(27) (a) Munha, R. F.; Zarkesh, R. A.; Heyduk, A. F. *Inorg. Chem.* **2013**, *52*, 11244−11255. (b) Murdock, K. C.; Lin, Y.-I.; Thomas, J. P.; Lang, S. A., Jr. *J. Med. Chem.* **1978**, *21*, 403−405.

DOI: 10.1021/acs.inorgchem.5b01380
Inorg. Chem. XXXX, XXX, XXX−XXX

(28) Sheldrick, G. M. *Acta Crystallogr., Sect. A: Found. Crystallogr.* **2008**, *64*, 112−122.
(29) Dolomanov, O. V.; Bourhis, L. J.; Gildea, R. J.; Howard, J. A. K.; Puschmann, H. *J. Appl. Crystallogr.* **2009**, *42*, 339−341.
(30) Neese, F. *ORCA-An Ab Initio, DFT and Semiempirical Electronic Structure Package*, version 2.9; Max Planck Institute for Bioinorganic Chemistry: Muelheim, Germany, 2012.
(31) (a) Becke, A. D. *J. Chem. Phys.* **1986**, *84*, 4524−4529. (b) Perdew, J. P. *Phys. Rev. B: Condens. Matter Mater. Phys.* **1986**, *33*, 8822−8824.
(32) (a) Becke, A. D. *J. Chem. Phys.* **1993**, *98*, 5648−5652. (b) Lee, C. T.; Yang, W. T.; Parr, R. G. *Phys. Rev. B: Condens. Matter Mater. Phys.* **1988**, *37*, 785−789.
(33) (a) Schafer, A.; Huber, C.; Ahlrichs, R. *J. Chem. Phys.* **1994**, *100*, 5829−5835. (b) Schafer, A.; Horn, H.; Ahlrichs, R. *J. Chem. Phys.* **1992**, *97*, 2571−2577. (c) Weigend, F.; Ahlrichs, R. *Phys. Chem. Chem. Phys.* **2005**, *7*, 3297−3305.
(34) Klamt, A.; Schueuermann, G. *J. Chem. Soc., Perkin Trans. 2* **1993**, 799−805.
(35) (a) Noodleman, L. *J. Chem. Phys.* **1981**, *74*, 5737−5743. (b) Sinnecker, S.; Neese, F.; Noodleman, L.; Lubitz, W. *J. Am. Chem. Soc.* **2004**, *126*, 2613−2622.
(36) Laaksonen, L. *J. Mol. Graphics* **1992**, *10*, 33.
(37) Addison, A. W.; Rao, T. N.; Reedijk, J.; Vanrijn, J.; Verschoor, G. C. *J. Chem. Soc., Dalton Trans.* **1984**, 1349−1356.
(38) (a) Marshak, M. P.; Chambers, M. B.; Nocera, D. G. *Inorg. Chem.* **2012**, *51*, 11190−11197. (b) Kolchinski, A. G.; Korybut-Daszkiewicz, B.; Rybak-Akimova, E. V.; Busch, D. H.; Alcock, N. W.; Clase, H. J. *J. Am. Chem. Soc.* **1997**, *119*, 4160−4171. (c) Szalda, D. J.; Schwarz, C. L.; Endicott, J. F.; Fujita, E.; Creutz, C. *Inorg. Chem.* **1989**, *28*, 3214−3219.
(39) (a) Eerdun, C.; Hisanaga, S.; Setsune, J.-i. *Chem. - Eur. J.* **2015**, *21*, 239−246. (b) Magdesieva, T. V.; Levitskiy, O. A.; Grishin, Y. K.; Ambartsumyan, A. A.; Paseshnichenko, K. A.; Kolotyrkina, N. G.; Kochetkov, K. A. *Organometallics* **2014**, *33*, 4639−4654. (c) Eerdun, C.; Hisanaga, S.; Setsune, J.-i. *Angew. Chem., Int. Ed.* **2013**, *52*, 929−932. (d) Soloshonok, V. A.; Ono, T.; Ueki, H.; Vanthuyne, N.; Balaban, T. S.; Burck, J.; Fliegl, H.; Klopper, W.; Naubron, J.-V.; Bui, T. T. T.; Drake, A. F.; Roussel, C. *J. Am. Chem. Soc.* **2010**, *132*, 10477−10483. (e) Constable, E. C. *Chem. Soc. Rev.* **2013**, *42*, 1637−1651. (f) Baum, G.; Constable, E. C.; Fenske, D.; Housecroft, C. E.; Kulke, T.; Neuburger, M.; Zehnder, M. *Dalton* **2000**, 945−959. (g) Mamula, O.; von Zelewsky, A. *Coord. Chem. Rev.* **2003**, *242*, 87−95. (h) Murner, H.; von Zelewsky, A.; Hopfgartner, G. *Inorg. Chim. Acta* **1998**, *271*, 36−39.
(40) (a) Kaim, W. *Coord. Chem. Rev.* **1987**, *76*, 187−235. (b) Coombe, V. T.; Heath, G. A.; MacKenzie, A. J.; Yellowlees, L. J. *Inorg. Chem.* **1984**, *23*, 3423−3425. (c) Braterman, P. S.; Song, J. I.; Peacock, R. D. *Inorg. Chem.* **1992**, *31*, 555−559.
(41) England, J.; Scarborough, C. C.; Weyhermueller, T.; Sproules, S.; Wieghardt, K. *Eur. J. Inorg. Chem.* **2012**, *2012*, 4605−4621.
(42) (a) Wang, M.; Weyhermueller, T.; Wieghardt, K. *Chem. - Eur. J.* **2014**, *20*, 9037−9044. (b) Wang, M.; England, J.; Weyhermueller, T.; Wieghardt, K. *Inorg. Chem.* **2014**, *53*, 2276−2287. (c) Wang, M.; England, J.; Weyhermueller, T.; Kokatam, S.-L.; Pollock, C. J.; DeBeer, S.; Shen, J.; Yap, G. P. A.; Theopold, K. H.; Wieghardt, K. *Inorg. Chem.* **2013**, *52*, 4472−4487. (d) Bowman, A. C.; England, J.; Sproules, S.; Weyhermuller, T.; Wieghardt, K. *Inorg. Chem.* **2013**, *52*, 2242−2256. (e) Scarborough, C. C.; Wieghardt, K. *Inorg. Chem.* **2011**, *50*, 9773−9793. (f) Scarborough, C. C.; Sproules, S.; Weyhermueller, T.; DeBeer, S.; Wieghardt, K. *Inorg. Chem.* **2011**, *50*, 12446−12462.
(43) (a) Davidson, J. J.; DeMott, J. C.; Douvris, C.; Fafard, C. M.; Bhuvanesh, N.; Chen, C.-H.; Herbert, D. E.; Lee, C.-I.; McCulloch, B. J.; Foxman, B. M.; Ozerov, O. V. *Inorg. Chem.* **2015**, *54*, 2916−2935. (b) Vreeken, V.; Siegler, M. A.; de Bruin, B.; Reek, J. N. H.; Lutz, M.; van der Vlugt, J. I. *Angew. Chem., Int. Ed.* **2015**, *54*, 7055−7059.
(44) Wanniarachchi, S.; Liddle, B. J.; Toussaint, J.; Lindeman, S. V.; Bennett, B.; Gardinier, J. R. *Dalton Trans.* **2011**, *40*, 8776−8787.
(45) (a) Allard, M. M.; Sonk, J. A.; Heeg, M. J.; McGarvey, B. R.; Schlegel, H. B.; Verani, C. N. *Angew. Chem., Int. Ed.* **2012**, *51*, 3178−3182. (b) Allard, M. M.; Xavier, F. R.; Heeg, M. J.; Schlegel, H. B.; Verani, C. N. *Eur. J. Inorg. Chem.* **2012**, *2012*, 4622−4631. (c) Lanznaster, M.; Hratchian, H. P.; Heeg, M. J.; Hryhorczuk, L. M.; McGarvey, B. R.; Schlegel, H. B.; Verani, C. N. *Inorg. Chem.* **2006**, *45*, 955−957. (d) Imbert, C.; Hratchian, H. P.; Lanznaster, M.; Heeg, M. J.; Hryhorczuk, L. M.; McGarvey, B. R.; Schlegel, H. B.; Verani, C. N. *Inorg. Chem.* **2005**, *44*, 7414−7422.
(46) (a) Pantazis, D. A.; Krewald, V.; Orio, M.; Neese, F. *Dalton Trans.* **2010**, *39*, 4959−4967. (b) Sandala, G. M.; Noodleman, L. *Methods Mol. Biol.* **2011**, *766*, 293−312.
(47) (a) Yamaguchi, K.; Takahara, Y.; Fueno, T. In *Applied Quantum Chemistry*; Smith, V. H., Ed.; Reidel: Dordrecht, 1986; p 155. (b) Soda, T.; Kitagawa, Y.; Onishi, T.; Takano, Y.; Shigeta, Y.; Nagao, H.; Yoshioka, Y.; Yamaguchi, K. *Chem. Phys. Lett.* **2000**, *319*, 223−230.
(48) Jones, R. D.; Summerville, D. A.; Basolo, F. *Chem. Rev.* **1979**, *79*, 139−179.
(49) To the best our knowledge, the only other complex with a single diarylamido bridge was reported in the following manuscript: Smith, D. A.; Ozerov, O. V. *Chem. Commun.* **2011**, *47*, 10779−10781.

DOI: 10.1021/acs.inorgchem.5b01380
Inorg. Chem. XXXX, XXX, XXX−XXX